



## OPEN ACCESS

## EDITED BY

Yiliang Li,  
The University of Hong Kong, Hong Kong,  
SAR China

## REVIEWED BY

Xiao Wu,  
Chinese Academy of Sciences, China  
Hongchen Jiang,  
China University of Geosciences Wuhan,  
China

## \*CORRESPONDENCE

Jon Telling,  
✉ jon.telling@newcastle.ac.uk

## †PRESENT ADDRESS

Jordan Stone,  
Department of Earth Science and  
Engineering, Imperial College London,  
London, United Kingdom

RECEIVED 06 March 2023

ACCEPTED 02 May 2023

PUBLISHED 23 May 2023

## CITATION

Stone J, Edgar JO, Rutherford J,  
Gill-Olivas B, Tranter M, Gould JA,  
Xavier CM and Telling J (2023), Flash  
heating boosts the potential for  
mechanochemical energy sources for  
subglacial ecosystems.  
*Front. Geochem.* 1:1180893.  
doi: 10.3389/fgeoc.2023.1180893

## COPYRIGHT

© 2023 Stone, Edgar, Rutherford, Gill-  
Olivas, Tranter, Gould, Xavier and Telling.  
This is an open-access article distributed  
under the terms of the [Creative  
Commons Attribution License \(CC BY\)](#).  
The use, distribution or reproduction in  
other forums is permitted, provided the  
original author(s) and the copyright  
owner(s) are credited and that the original  
publication in this journal is cited, in  
accordance with accepted academic  
practice. No use, distribution or  
reproduction is permitted which does not  
comply with these terms.

# Flash heating boosts the potential for mechanochemical energy sources for subglacial ecosystems

Jordan Stone<sup>1†</sup>, John O. Edgar<sup>1</sup>, Johnny Rutherford<sup>1</sup>,  
Beatriz Gill-Olivas<sup>2</sup>, Martyn Tranter<sup>3</sup>, Jamie A. Gould<sup>4</sup>,  
Cijo M. Xavier<sup>4</sup> and Jon Telling<sup>1\*</sup>

<sup>1</sup>School of Natural and Environmental Sciences, Newcastle University, Newcastle Upon Tyne, United Kingdom, <sup>2</sup>Bristol Glaciology Centre, University of Bristol, Bristol, United Kingdom, <sup>3</sup>ENVS, Aarhus University, Risø, Denmark, <sup>4</sup>Faculty of Science, Agriculture & Engineering, Newcastle University, Newcastle Upon Tyne, United Kingdom

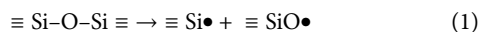
Subglacial environments harbour a diversity of microbial ecosystems capable of influencing biogeochemical cycles. However, the darkness and isolation of subglacial environments limit the energy sources available for microbial metabolism. A recently recognised energy source for these microbes in wet-based regions is the rock-water reactions that occur after the mechanical fracturing of glacial bedrock. These mechanochemical reactions produce H<sub>2</sub> and H<sub>2</sub>O<sub>2</sub> at 0°C from reactions with mineral surface defects (Si• and SiO•) and release Fe from within the mineral structures, providing electron donors and acceptors for microbial metabolism. However, the production of H<sub>2</sub>O<sub>2</sub> and H<sub>2</sub> may be underestimated as temperatures at rock abrasion sites can increase substantially above 0°C as glaciers “slip and grind” rocks, potentially accelerating the rates of mechanochemical reactions. Despite this, the effect of rapid heating on subsequent low-temperature mechanochemical reactions has yet to be examined. Here, we investigate H<sub>2</sub>, H<sub>2</sub>O<sub>2</sub>, and Fe production during low-temperature (0 °C) incubations of water with a range of ground rocks and minerals following “flash heating” to 30, 60, or 121 °C. We show that transient increases (as little as 5–10 min of heating) to moderate temperatures (30 or 60 °C) can significantly increase the rate of H<sub>2</sub> production, while short-term heating to 121 °C generates larger bursts of H<sub>2</sub>. In addition, pyrite is easily crushed, potentially releasing large quantities of Fe<sup>2+</sup> into subglacial systems and promoting mechanochemical reactions due to the resulting large surface area (10× larger than other materials). We provide the first evidence for H<sub>2</sub> production from water reactions with crushed pyrite and suggest that crushed pyrite has a greater influence on subglacial H<sub>2</sub>O<sub>2</sub> production than silicates. We conclude that electron donors in the form of Fe<sup>2+</sup> and H<sub>2</sub> bursts can be produced in subglacial ecosystems, which may be coupled to substantial concentrations of H<sub>2</sub>O<sub>2</sub> produced from crushed pyrite. This suggests that rock–water mechanochemical reactions may be a greater source of energy for subglacial environments than previously recognised.

## KEYWORDS

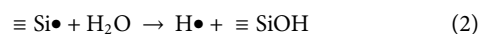
hydrogen, hydrogen peroxide, subglacial, microbial, temperature, mechanochemistry, energy

## 1 Introduction

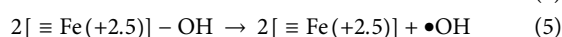
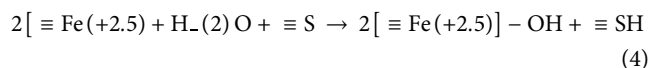
Understanding how microbes survive in cold subsurface environments under conditions of darkness, isolation, high pressure, and low temperature has garnered increasing attention (Wadham et al., 2008; Christner et al., 2014; Gill-Olivas et al., 2021). However, the ubiquitous presence of rock comminution (e.g., from rock grinding at the glacier bed) and water in cold subsurface environments indicates that rock–water reactions may be prevalent (Telling et al., 2015; Gill Olivas, 2019). Silicon-oxygen bonds are broken by rock comminution, resulting in the formation of Si• and SiO• (Kita et al., 1982; Fubini et al., 1990; He et al., 2021; Eq. 1).



Si• reacts with water at 0 °C to produce H<sub>2</sub> gas over hours to weeks (Telling et al., 2015; Eq. 2; Eq. 3), providing energy to subglacial ecosystems and supporting methanogenesis (Telling et al., 2015; Macdonald et al., 2018; Parkes et al., 2019).



The potential for additional energy supplied from mechanochemically produced H<sub>2</sub>O<sub>2</sub> as an electron acceptor coupled to H<sub>2</sub> has recently been identified (Gill-Olivas et al., 2021). Pyrite is a potentially large source of H<sub>2</sub>O<sub>2</sub> in subglacial environments, even in the absence of O<sub>2</sub> (Gill-Olivas et al., 2021). The mechanism of H<sub>2</sub>O<sub>2</sub> production at the surface remains controversial, but it involves the reaction of H<sub>2</sub>O or O<sub>2</sub> with the Fe<sup>3+</sup> and sulfur-deficient sites on the fractured pyrite surface (Xian et al., 2019; Borda et al., 2003; e.g., through Eq. 4 and Eq. 5). The process generates •OH as an intermediate, which combines to form H<sub>2</sub>O<sub>2</sub> (Eq. 6).



However, despite the linking of Fe<sup>2+</sup> to H<sub>2</sub> production (McCollom and Bach, 2009; Irfan et al., 2019), no study has examined the production of H<sub>2</sub> from reactions of water with crushed pyrite (a mineral with high Fe<sup>2+</sup> content). If crushed pyrite can produce H<sub>2</sub> in addition to the substantial quantities of H<sub>2</sub>O<sub>2</sub> indicated by Gill-Olivas et al. (2021), then the energy available from mechanochemical reactions in cold subsurface environments may be much higher than previously estimated.

The rate of mechanochemical H<sub>2</sub> production typically increases with temperature up to ~90 °C - within the range of microbial habitability (Kita et al., 1982; Parkes et al., 2019; Stone et al., 2022) - reducing the potential for H<sub>2</sub> production in colder environments. However, the cold subsurface biosphere experiences fluctuating temperatures that can impact the chemistry of energy-providing rock–water reactions. For example, certain glaciers can exhibit “stick–slip” behaviour where energy is built up as glaciers “stick” to rough ground and is then released (up to 4 W/m<sup>2</sup> of frictional heating—Benn et al., 2019) during a “slip” (Fischer and Clarke, 1997; Sevestre and Benn, 2015). The increased sliding velocity during a slip can increase bedrock erosion (Fischer et al., 2013; Cook et al., 2020) and generate high spot temperatures

(Zhang and Valentine, 2002). The temperatures reached are difficult to observe in the field, but, based on an approximate calculation, spot temperatures can be as high as 155 °C (Supplementary Material S1.2.2). Such high transitory temperatures can locally increase the rate of mechanochemical reactions (Figure 1) and boost the potential for H<sub>2</sub> production in low-temperature environments. In addition, the potential activation of SiO• at high temperatures can stimulate H<sub>2</sub>O<sub>2</sub> production (Eq. 7; Eq. 5) or inhibit H<sub>2</sub> production (Eq. 8 outcompetes Eq. 3; Stone et al., 2022; Gill-Olivas et al., 2021).



Fe<sup>2+</sup> may also be generated from crushed rocks and minerals. The effect of the resulting Fenton reactions (due to Fe<sup>2+</sup> and H<sub>2</sub>O<sub>2</sub>; Fenton, 1894) on mechanochemically derived energy and H<sub>2</sub> has yet to be studied. For example, by generating highly reactive •OH (Araujo et al., 2011; Eq. 9):



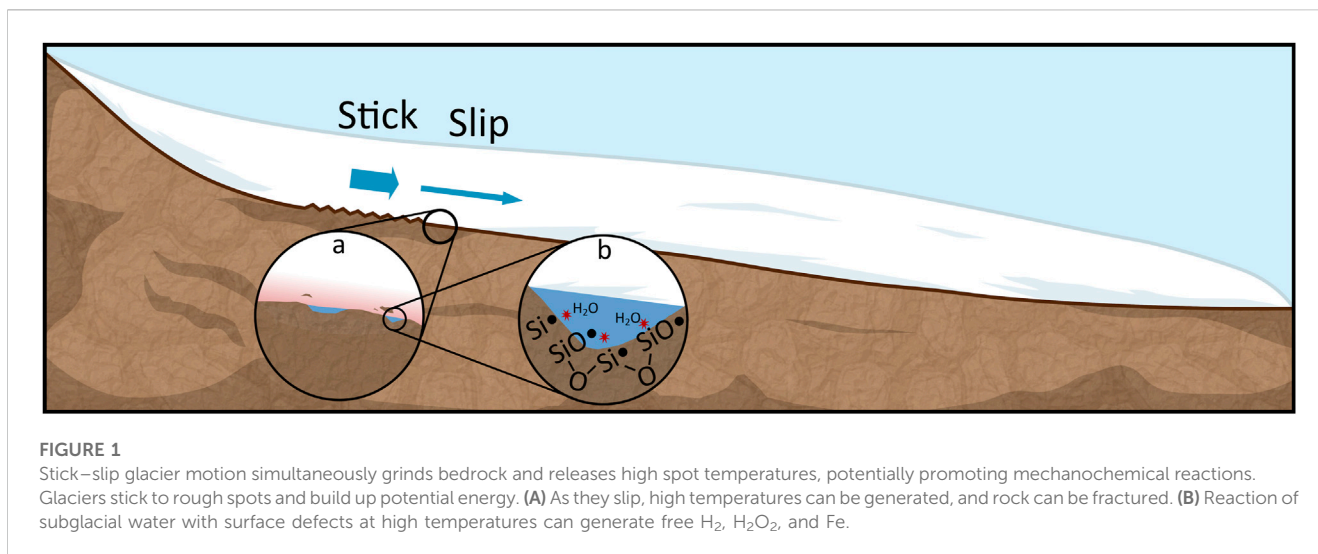
In addition, if Fe<sup>2+</sup> is generated in large quantities, it may serve as an electron donor to couple with O<sub>2</sub>, including any O<sub>2</sub> generated from H<sub>2</sub>O<sub>2</sub> via the action of catalase (Kayani et al., 2018). Furthermore, it is possible (although not currently documented *in situ*) that some microorganisms may be able to use H<sub>2</sub>O<sub>2</sub> directly as a terminal electron acceptor using the cytochrome-c peroxidase as a respiratory oxidase (Khademian and Imlay, 2017).

This study aims to investigate low-temperature rock–water reactions, following short-term (hereafter referred to as “flash”) heating. A range of rocks and minerals, representing a mix of subglacial sediments, were ground in a planetary ball mill under anoxic conditions. H<sub>2</sub>O<sub>2</sub>, H<sub>2</sub>, and Fe were measured due to their potential impact on subglacial microbial communities and to build on past research on mechanochemical reactions. Rock and mineral powders were added to 0 °C anoxic water, rapidly heated to 30, 60, or 121 °C, and incubated at 0 °C for 1 h, 1 day, and 1 week. Concentrations of H<sub>2</sub>, H<sub>2</sub>O<sub>2</sub>, and aqueous iron were measured at each time point.

## 2 Materials and methods

### 2.1 Rock and mineral milling

All rocks and minerals were commercially sourced from Northern Geological Supplies Limited (Bolton, United Kingdom). Initially, quartz (cat# RckCryChnKBg; a common mineral that has been used in extensive mechanochemistry research—e.g., Fubini et al., 1987), basalt (cat# bas1 kg; a major rock of the oceanic crust), granite (cat# gasg1 kg; a major rock of the continental crust that produces high quantities of H<sub>2</sub>—Parkes et al., 2011; Telling et al., 2015), and pyrite (cat# PyrKbg; common in subglacial systems and capable of generating H<sub>2</sub>O<sub>2</sub>—Borda et al., 2001; Gill-Olivas et al., 2021) were crushed with a sledgehammer on an anvil (washed with 100% ethanol) inside multiple thick polyethylene bags. The materials were then crushed with a jaw crusher (after an initial discard) and sieved to a uniform 1–3 mm size fraction. They were then sieved again, washed in 18.2 MΩ cm<sup>-1</sup> water, and ultrasonicated to remove fine dust particles. The materials were



then dried at 60 °C for >1 week before milling and crushed in a planetary ball mill. The planetary ball mill was cleaned twice by milling with pure quartz and once with the desired material for 2 min each before crushing the experimental sample. Due to the limited size of the mortar, the planetary ball mill was run twice with 45 g of material each time. The mortar was sealed with a Viton O-ring and enclosed within a custom-made stainless-steel tri-axial clamping system. The ball mill was then vacuumed and flushed with N<sub>2</sub> for seven cycles before the N<sub>2</sub> headspace was equilibrated to atmospheric pressure using a syringe (Kaur et al., 2016; Gill-Olivas et al., 2021). Each milling was performed at 500 rpm for 30 min (Telling et al., 2015; Gill-Olivas et al., 2021). Prior tests have demonstrated that, under these conditions, contamination of agate from the ball mill or grinding balls into the crushed rock or mineral sample is ≤0.2% (Stone et al., 2022). The ball mill was then transferred and opened into a glove bag filled and continuously flushed with 5.0 grade N<sub>2</sub> (<10 ppm O<sub>2</sub>). The O<sub>2</sub> within the glove bag was also confirmed to be <0.1% O<sub>2</sub> using a PreSens optical O<sub>2</sub> sensor. We then transferred 2 g (1.94–2.05 g) subfractions into 10-mL borosilicate serum vials (previously autoclaved, bathed in 10% HCl for 2 h, rinsed in 18.2 MΩ cm<sup>-1</sup> water, and furnace at 500 °C for 4 h—Parkes et al., 2011; Telling et al., 2015). Vials were sealed with thick butyl rubber stoppers (previously autoclaved at 121 °C for 30 min, boiled in 1 M NaOH for 1 h (McCollom and Donaldson, 2016), rinsed in 18.2 MΩ cm<sup>-1</sup> water, and dried under a fume hood), and crimp sealed. The remaining material was stored at room temperature in a sealed plastic tub for grain size analysis. Blank controls were treated identically but without the rock/mineral powder. The vials were then flushed with N<sub>2</sub> for 2 min each to remove any trace O<sub>2</sub> and then equilibrated to 1 atm (Telling et al., 2015; Gill-Olivas et al., 2021).

## 2.2 Water preparation and addition

De-oxygenated water was prepared by autoclaving 18.2 MΩ cm<sup>-1</sup> water in a 0.5 L borosilicate Duran bottle at 121 °C for 1 h. The Duran bottle was then placed in a 0 °C water bath and

vigorously bubbled with N<sub>2</sub> for ~4 h; dissolved O<sub>2</sub> was measured to be 0.216 mg L<sup>-1</sup> (equivalent to 6.74 μmol L<sup>-1</sup>) with a calibrated PreSens O<sub>2</sub> optical sensor. We then added 4 mL of deoxygenated water to each vial (~2 h after crushing) using a gas-tight syringe and needle, which were shaken for 10 s.

## 2.3 Heating and sampling

Vials were stored in a 0 °C water bath for 5–30 min before heating. Batches of nine vials were either kept at 0 °C or rapidly flash-heated to 30 °C (water bath), 60 °C (oven), or 121 °C (autoclave) for 1 min; the vials were then rapidly cooled in the dark at 0 °C (see Stone et al., 2022). The temperature was measured using a vial with a temperature probe (held in place using aluminium foil) in 4 mL of water. Triplicate vials were then destructively sampled at 1 h, 24 h, and 168 h. During sampling, 4 mL gas (replaced with N<sub>2</sub>) was taken and stored at an overpressure in 3 mL Exetainers with double-wadded caps (evacuated to <0.6 mbar) using a gastight syringe and needle for later H<sub>2</sub> analysis (Telling et al., 2015). The vial was then shaken to ensure that the liquid was homogeneous (Telling et al., 2015), and a 2 mL liquid sample was extracted using a syringe and needle for H<sub>2</sub>O<sub>2</sub> and Fe<sup>2+</sup> analysis.

## 2.4 H<sub>2</sub> generation

H<sub>2</sub> was measured using a ThermoFisher gas chromatograph with a helium pulsed discharge detector (GC-PDD) with a 2-m micro-packed Shin Carbon ST 100/120 mesh, 1/16-inch OD, and 1.0 mm ID column, with a constant flow (10 mL<sup>-1</sup>) of helium carrier gas and a run time of 12.5 min. The column temperature was 60 °C, the injector temperature was 110 °C, and the detector temperature was 110 °C. Samples were calibrated against certified (±5%) 100 ppm standards (BOC). Three standards were run daily throughout the experimental period (coefficient of variation = 5.97%, n = 39). We injected 100 μL of gas from Exetainers directly into the column of the GC. The ideal gas law was used to calculate the mol H<sub>2</sub> in the

headspace of the vials from the ppm concentration (Okland et al., 2014). Adjustments were made for dilution during sampling, and the mol H<sub>2</sub> was normalised to dry material weight.

## 2.5 H<sub>2</sub>O<sub>2</sub> detection

H<sub>2</sub>O<sub>2</sub> concentrations were analysed immediately after sampling using a UV-spectrophotometric method (Baga et al., 1988; Borda et al., 2001). The method measures the quantity of copper (I)–DMP complex (Cu(DMP)<sup>2+</sup>) formed in the presence of H<sub>2</sub>O<sub>2</sub> at a wavelength of 454 nm after a reaction time of ~20 min. Daily standards were prepared from a stock solution of 1000 μmol L<sup>-1</sup> H<sub>2</sub>O<sub>2</sub> to prevent the photodegradation of H<sub>2</sub>O<sub>2</sub> (Ueki et al., 2020; Yi et al., 2012; coefficient of variation = 0.03%, n=12).

## 2.6 Fe detection

Ferrozine spectrophotometry was used to measure Fe<sup>2+</sup> and Fe<sup>3+</sup> in the liquid samples (Viollier et al., 2000; Stone et al., 2022). This method determines the concentration of Fe<sup>2+</sup> based on the measurement of the Fe<sup>2+</sup>-ferrozine complex formed by the reaction of Fe<sup>2+</sup> with ferrozine. The use of a reducing agent, hydroxylamine hydrochloride, allows the measurement of Fe<sup>3+</sup> concentration (Viollier et al., 2000). Samples were stored in evacuated Exetainers for <2 weeks prior to analysis, and were analysed in the open air (exposing them to air for 5–20 min during analysis). Under similar conditions, a pH range of 7–10 was recorded by Stone et al. (2022).

## 2.7 Grain size analysis

The grain size was measured by laser diffraction using a Mastersizer 3000 with Mastersizer v3.81 software, with 15 replicates per analysis. Three separate samples of the material that remained after milling were added to the Mastersizer at 10%–20% obscuration with five replicates each.

## 2.8 Surface area analysis

The surface area of the materials was measured using a NOVA 1200e BET Analysis System. Approximately 1 g of dried crushed mineral was loaded into a pre-calibrated sample cell. The entire system was then evacuated and dried at 300 °C for 2 h (Bardestani et al., 2019). The surface area of the materials was measured using nitrogen gas as an adsorbent at 77 K.

## 2.9 Mineral phase identification

Six-phase identification was performed by XRD using a PANalytical X'Pert Pro MPD, powered using a Philips PW3040/60 X-ray generator fitted with an X'Celerator detector. Powder samples were exposed to Cu-Kα X-rays at a characteristic wavelength (λ) of 1.5418 Å to generate diffraction data. A Cu anode supplied with 40 kV and a current of 40 mA was used to

acquire X-ray data. Using a scanning X'Celerator detector and a secondary Ni monochromator in the diffracted beam path, the data sets were collected over the range 5°–100° 2θ with a step size of 0.0334° 2θ and a nominal time per step of 1 s. The optics were set up with an incident anti-scatter slit of 4°, a programmable divergence slit with a fixed length of 10 mm, a beam mask of 20 mm, and incident/diffracted Soller slits of 0.04 radians. Scans were performed in continuous mode. Data were exported as XRDML files, and profiles were fitted using a minimum second derivative method and evaluated by searching the Crystallography Open Database (COD; <http://www.crystallography.net/cod/>) using Malvern Panalytical HighScore Plus software. The mineral search was restricted to phases containing at least one of the major elements O, Si, Al, Fe, Mg, Na, K, and Ca and potentially containing Ti, Mn, Ni, S, and Cl. The Reitveld method was used to further analyse the data; this involves constructing a model consisting of the crystal structures of all component phases; the differences between the observed and simulated diffraction patterns are minimised by varying the scale factors, unit-cell parameters, and crystallite size for each phase. This method provides information about well-ordered (crystalline) phases.

## 2.10 Data analysis and presentation

All concentrations were normalised to dry sediment mass (μmol g<sup>-1</sup>). Detection limits were calculated based on the sum of the mean of the blanks and the standard deviation multiplied by three. Statistical analyses were conducted using IBM SPSS Statistics 25., Mann-Whitney U tests were used to test whether each temperature and time point was significantly different from the blanks (*p*<0.05; two-tailed). Independent sample t-tests (*p*<0.05; two-tailed) were used to determine whether there were differences in the chemistry of larger groups. One-way ANOVA (two-tailed) was used to test for significant differences in H<sub>2</sub> and H<sub>2</sub>O<sub>2</sub>. Spearman's rank was used to evaluate the relationships between different molecules, time, and temperature (*p*<0.05; two-tailed). Oxygen mass balance calculations were conducted as per Stone et al. (2022) (Supplementary Material S1.2.1).

# 3 Results

## 3.1 Rock and mineral crushing

Equal crushing time and intensity produced varied grain sizes and surface areas depending on the material. Pyrite had the smallest grain size (4.1 μm) and the largest surface area (26.2 m<sup>2</sup> g<sup>-1</sup>). Granite, quartz, and basalt had grain sizes ranging from 16.8 to 27.0 μm (Supplementary Figure S1) and surface areas ranging from 2.3 to 3.0 m<sup>2</sup> g<sup>-1</sup> (Supplementary Table S1). Mineral phase identification is presented in Supplementary Tables S1, S5.

## 3.2 Hydrogen generation

The results for 24 h showed a significant increase in H<sub>2</sub> production from crushed granite and pyrite after flash heating to 30 or 60 °C (T-test: *t*<sub>18,01</sub> = -3.696, *p* = 0.002); H<sub>2</sub> production from pyrite only differed significantly from the blanks after flash heating to 30 or 60 °C

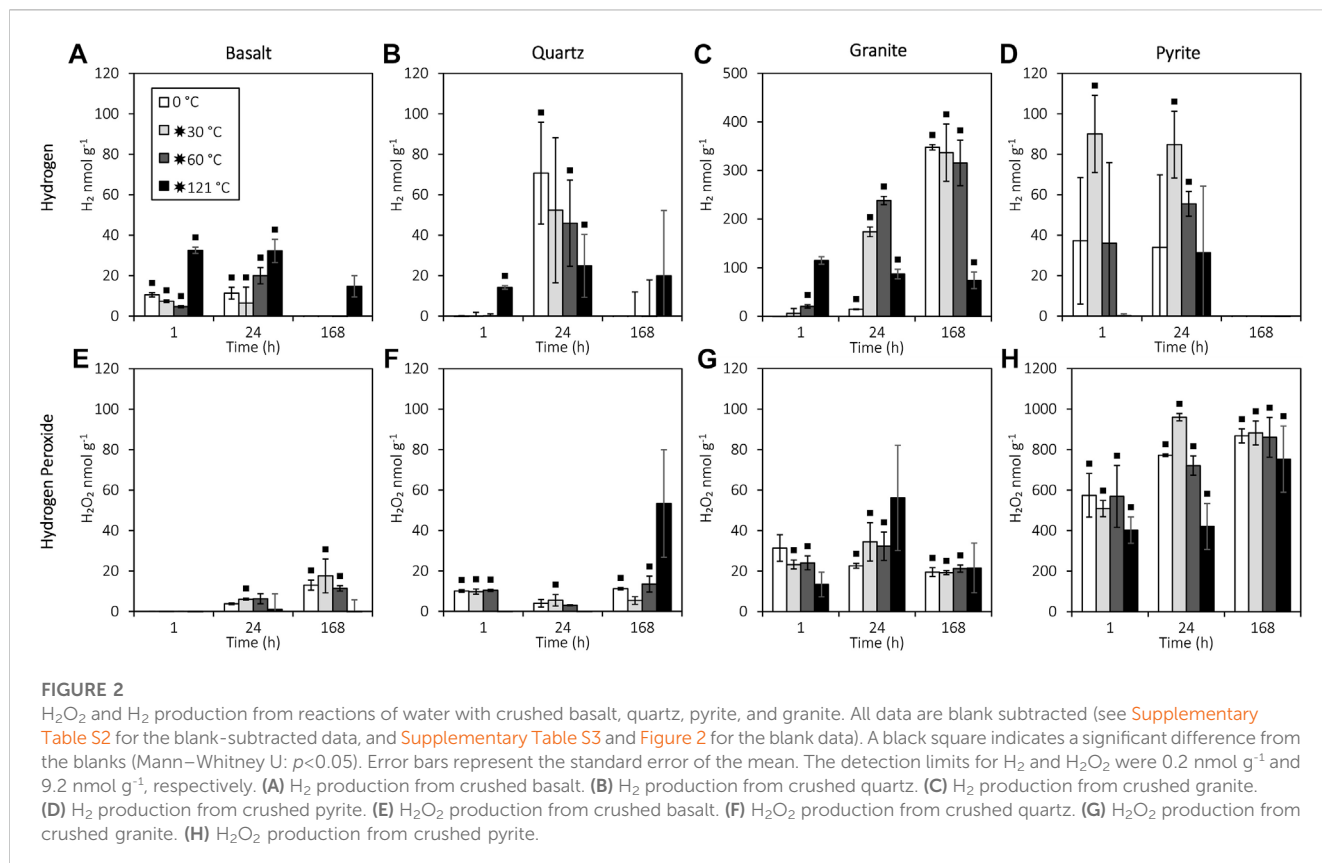


([Figure 2C](#)). In addition, flash heating to  $121^\circ\text{C}$  caused an initial burst of  $\text{H}_2$  production after 1 h from basalt (ANOVA:  $F_{3,8}=41$ ,  $p < 0.001$ ; LSD:  $p < 0.001$ ), quartz (ANOVA:  $F_{3,8}=34.388$ ,  $p < 0.001$ ; LSD:  $p < 0.001$ ), and granite (ANOVA:  $F_{3,7}=60.178$ ,  $p < 0.001$ ; LSD:  $p < 0.001$ ). However, after 24 h, granite that was flash heated to  $121^\circ\text{C}$  showed significantly lower  $\text{H}_2$  production than  $30^\circ\text{C}$  and  $60^\circ\text{C}$  (ANOVA:  $F_{3,20}=3.727$ ,  $p = 0.028$ ; LSD:  $p = 0.014$ ,  $p = 0.007$ , respectively), while basalt and quartz showed no significant  $\text{H}_2$  production 1 week after flash heating to  $121^\circ\text{C}$  ([Figures 2A, B](#)). The  $\text{H}_2$  concentration decreased between 24 and 168 h for quartz (t-test:  $t_{22}=3.64$ ,  $p = 0.001$ ), basalt (t-test:  $t_{22}=4.66$ ,  $p < 0.001$ ), and pyrite (t-test:  $t_{16,887}=7.434$ ,  $p < 0.001$ ), with all  $\text{H}_2$  initially generated from pyrite reduced to below detection after 1 week ([Figure 2C](#)).

### 3.3 Hydrogen peroxide generation

Pyrite produced significantly more  $\text{H}_2\text{O}_2$  than the silicates (t-test:  $t_{35,181}=-18.066$ ,  $p < 0.001$ ) and produced an order of magnitude more  $\text{H}_2\text{O}_2$  than  $\text{H}_2$  (reaching  $391 \mu\text{mol L}^{-1} \text{H}_2\text{O}_2$ ; [Figure 2G](#)). However, unlike  $\text{H}_2$  production, flash heating to 30 or  $60^\circ\text{C}$  did not significantly affect  $\text{H}_2\text{O}_2$  production from granite, basalt, or quartz compared to constant  $0^\circ\text{C}$  incubation (ANOVA:  $F_{2,78}=0.033$ ,  $p = 0.968$ ).  $\text{H}_2\text{O}_2$  concentrations were not related to  $\text{H}_2$  in the granite experiment (Spearman's:  $r_s = -0.172$ ,  $n = 35$ ,  $p = 0.322$ ), but  $\text{H}_2\text{O}_2$  and  $\text{H}_2$  were negatively correlated in the basalt (Spearman's:  $r_s = -0.535$ ,  $n = 36$ ,  $p = 0.001$ ), quartz (Spearman's:  $r_s = -0.409$ ,  $n = 36$ ,  $p = 0.013$ ), and pyrite (Spearman's:  $r_s = -0.386$ ,  $n = 36$ ,  $p = 0.020$ ) experiments.

### 3.4 Aqueous iron generation

Granite and basalt released detectable  $\text{Fe}^{3+}$  into the water, while pyrite released higher concentrations of  $\text{Fe}^{2+}$  and  $\text{Fe}^{3+}$ . Neither  $\text{Fe}^{2+}$  nor  $\text{Fe}^{3+}$  was significantly correlated (Spearman's:  $r_s = 0.123$ ,  $n = 36$ ,  $p = 0.475$ ;  $r_s = 0.140$ ,  $n = 36$ ,  $p = 0.415$ ) with  $\text{H}_2\text{O}_2$  concentration in the crushed pyrite experiment. Aqueous  $\text{Fe}^{2+}$  in pyrite experiments was not significantly correlated (Spearman's:  $r_s = 0.262$ ,  $n = 36$ ,  $p = 0.123$ ) with  $\text{H}_2$ . However,  $\text{Fe}^{2+}$  and  $\text{Fe}^{3+}$  were significantly correlated with each other (Spearman's:  $r_s = 0.640$ ,  $n = 36$ ,  $p < 0.001$ ; see [Supplementary Figure S3](#) for blanks) despite two orders of magnitude difference in their concentrations ([Figure 3](#)).  $\text{Fe}^{2+}$  and  $\text{Fe}^{3+}$  from crushed granite (Spearman's:  $r_s = -0.657$ ,  $n = 36$ ,  $p < 0.001$ ) and basalt (Spearman's:  $r_s = -0.735$ ,  $n = 36$ ,  $p < 0.001$ ) were also significantly correlated ([Figure 3](#)). Notably, all  $\text{Fe}^{2+}$  concentrations from the basalt, granite, and quartz experiments were lower than the blanks ([Figure 3](#)).

## 4 Discussion

### 4.1 $\text{H}_2$ and $\text{H}_2\text{O}_2$ generation from crushed silicates

Results for 24 h show that flash heating to 30 or  $60^\circ\text{C}$  increases  $\text{H}_2$  production from granite, consistent with the thermal activation of  $\text{Si}^\bullet$  ([Telling et al., 2015](#); [Parkes et al., 2019](#); Eq. 2; Eq. 3). Heating to only  $30^\circ\text{C}$  for 5 min ([Figure 2](#)) caused an order of magnitude increase in  $\text{H}_2$  production from crushed granite after 24 h (15 vs.  $174 \text{ nmol g}^{-1}$ ),

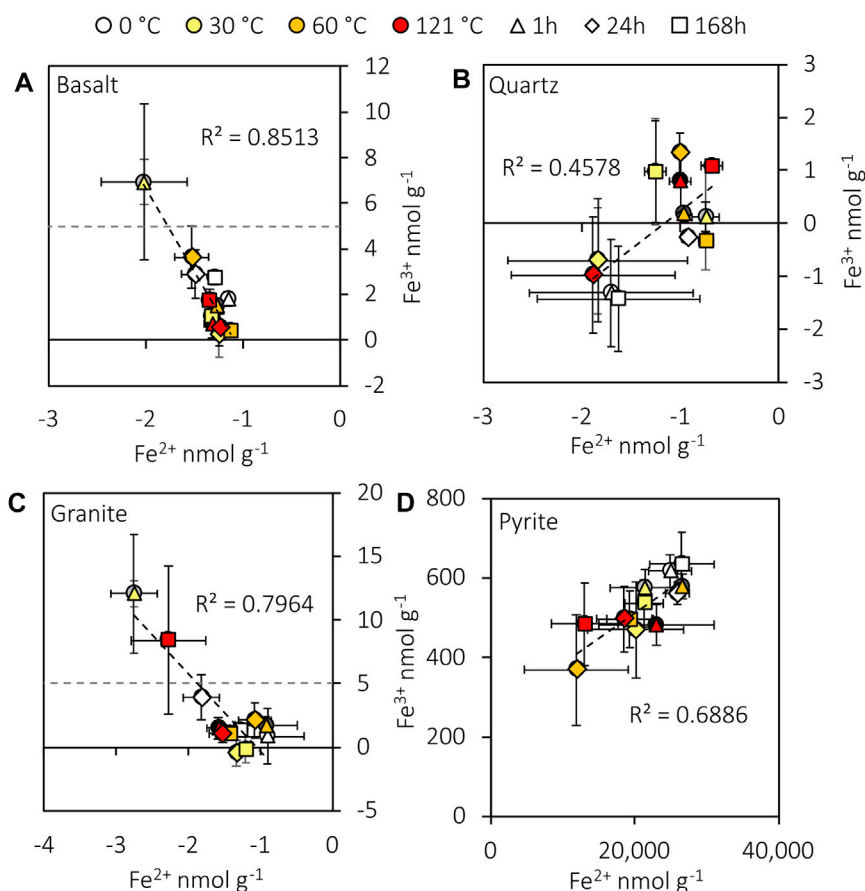


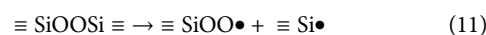
**FIGURE 3**

Plots of aqueous  $\text{Fe}^{2+}$  and  $\text{Fe}^{3+}$  generated from crushed basalt (A), quartz (B), granite (C), and pyrite (D). Data are blank subtracted. The experimental detection limits for  $\text{Fe}^{2+}$  and  $\text{Fe}^{3+}$  are 4 and 5  $\text{nmol g}^{-1}$ , respectively. The negative concentrations indicate a loss of Fe relative to the mean blank concentrations (see Supplementary Figure S3 for the blanks). Error bars represent the standard error of the mean.

indicating that even very temporary increases to modest temperatures have the capacity to promote faster  $\text{H}_2$  production from the reaction of  $\text{H}_2\text{O}$  with  $\text{Si}\bullet$ . Glacier slip can release  $4 \text{ W/m}^2$  of frictional heating (Benn et al., 2019), with the stick-slip events lasting up to 10–30 min (Bindschadler et al., 2003), suggesting that glaciers with stick-slip motion may have the potential to significantly boost subglacial  $\text{H}_2$  generation rates. Notably, after 1 week, the  $\text{H}_2$  production from a constant incubation at  $0^\circ\text{C}$  (no heating) had “caught up” to samples flash heated to  $30$  or  $60^\circ\text{C}$ , demonstrating that increased  $\text{H}_2$  production from flash heating to  $30$  or  $60^\circ\text{C}$  does not ultimately affect maximum  $\text{H}_2$  yield. Although the heat generated from stick-slip behaviour may not raise the bulk temperature of subglacial water by more than a fraction of a degree (Kita et al., 1982; Hart et al., 2011), the transient increase in the temperature of the mineral surface free radicals at rock abrasion sites (Figure 1) may potentially drive higher concentration bursts of  $\text{H}_2$  that could help support microbial communities (Telling et al., 2015). We recommend further experiments using shorter-duration temperatures to further test this hypothesis.

In addition,  $121^\circ\text{C}$  flash heating caused a burst of  $\text{H}_2$  production after 1 h (Figure 3) in all other silicates. However, the results for 168 h showed further inhibition of  $\text{H}_2$  production by  $121^\circ\text{C}$  flash heating of basalt and quartz. The maximum  $\text{H}_2$  yield

from granite at  $121^\circ\text{C}$  was also significantly ( $p < 0.05$ ) reduced compared to lower temperatures (Figure 3). The inhibition of  $\text{H}_2$  generation at  $121^\circ\text{C}$  is consistent with the reaction of  $\text{H}\bullet$  with  $\text{SiO}\bullet$  at high temperatures ( $>90^\circ\text{C}$ ; Stone et al., 2022; Eq. 8), resulting in the formation of  $\equiv\text{SiOH}$  at mineral surfaces instead of  $\text{H}_2$  generation (Eq. 2; Eq. 3; Kita et al., 1982). We noted, however, that, due to logistical constraints, temperatures  $> 90^\circ\text{C}$  were maintained for 40 min in the  $121^\circ\text{C}$  experiments, although such sustained temperature increases are highly unlikely during subglacial rock grinding. The inhibitory effect of this mechanism on *in situ* subglacial  $\text{H}_2$  generation yields may therefore be minimal. The high generation of  $\text{H}_2\text{O}_2$  (significantly higher than blank,  $p < 0.05$ ; Supplementary Material S1.1) at lower temperatures (Figure 3) most likely does not result from the reaction of  $\text{SiO}\bullet$  but ultimately from the more reactive  $\text{SiOO}\bullet$  that can be formed from trace  $\text{O}_2$  in the experiments (Eqs 10, 12 and 13; Kita et al., 1982; Stone et al., 2022) or from the homolytic cleavage of peroxy linkages (Eqs 11–13; He et al., 2023).





O<sub>2</sub> mass balance calculations (Supplementary Material S1.2.2) indicate that there was sufficient trace oxygen in the vials (235 nmol g<sup>-1</sup>) to explain the generation of SiOO• in sufficient quantities to produce the observed H<sub>2</sub>O<sub>2</sub> from crushed silicates (max of 56.1 nmol g<sup>-1</sup>). We suggest that, at 121 °C, no significant H<sub>2</sub>O<sub>2</sub> was generated by this mechanism as fewer Si• sites were available for reaction with O<sub>2</sub> due to faster reaction rates with H<sub>2</sub>O to generate H•, which were then consumed by reaction with activated SiO• sites (Kita et al., 1982). SiO• at higher temperatures may therefore inhibit some H<sub>2</sub>O<sub>2</sub> production in the presence of O<sub>2</sub>, although H<sub>2</sub>O<sub>2</sub> can still be generated by the homolytic cleavage of peroxy linkages (Si-O-O-Si). Additional small quantities of H<sub>2</sub>O<sub>2</sub> (and O<sub>2</sub>) may also have been produced independently of the existing O<sub>2</sub> by the reaction of water with SiO• at low temperatures. The SiO• may have been formed by the breakage of Si-O-Si bonds (Eq. 1, Eq. 5, Eq. 7) or the uniaxial stressing of peroxy linkages (Si-O-O-Si; He et al., 2021).

Fenton reactions are likely to have exerted additional controls on H<sub>2</sub>O<sub>2</sub> concentrations in the experiments (Fenton, 1894; Edgar et al., 2022). Aqueous Fe<sup>2+</sup> concentrations in the granite and basalt experiments were lower than the blanks in all experiments (Figure 3), consistent with the reaction of Fe<sup>2+</sup> with H<sub>2</sub>O<sub>2</sub>. In addition, there was a negative correlation between Fe<sup>2+</sup> and Fe<sup>3+</sup> from both crushed rocks (Figure 3), providing further evidence that Fe<sup>2+</sup> may have oxidised to Fe<sup>3+</sup>. In addition, H<sub>2</sub>O<sub>2</sub> and H<sub>2</sub> concentrations were negatively correlated in all experiments except the granite, suggesting that H<sub>2</sub>O<sub>2</sub> may also have reacted with H<sub>2</sub>. This may also have occurred indirectly through the generation of •OH from the Fenton reactions, which may have reacted with H<sub>2</sub> (Allen et al., 1952; Edgar et al., 2022). Therefore, the H<sub>2</sub>O<sub>2</sub> concentrations measured in these experiments (Figure 3) are likely to have underestimated the total H<sub>2</sub>O<sub>2</sub> production potential of crushed granite and basalt.

## 4.2 H<sub>2</sub>O<sub>2</sub> generation from crushed pyrite

H<sub>2</sub>O<sub>2</sub> concentrations produced from crushed pyrite (minimum 12 μmol g<sup>-1</sup>) greatly exceeded the estimated concentrations of O<sub>2</sub> in the experiments (0.2 μmol g<sup>-1</sup>). Therefore, while reactions of O<sub>2</sub> with the mineral surface may have contributed to ROS generation (Schoonen et al., 2010; Zhang et al., 2016), the majority of H<sub>2</sub>O<sub>2</sub> in these experiments seems to have come from a different source. The H<sub>2</sub>O<sub>2</sub> from the crushed pyrite experiments was likely generated by reactions of water with the crushed pyrite surface. Borda et al. (2003) outlined a mechanism involving the reaction of adsorbed H<sub>2</sub>O with Fe<sup>3+</sup> formed on the mineral surface (Eq. 4; Eq. 5). However, further investigations have questioned the thermodynamic feasibility of the oxidation of water at the Fe<sup>3+</sup> sites (Buckley and Woods, 2015). Instead, reactions of water with the mineral surface at sulfur-deficient sites may have been the predominant •OH generation pathway (Zhang et al., 2016; Xian et al., 2019). Therefore, the detailed reaction mechanisms at the pyrite surface remain unclear. Nevertheless, the 10× higher surface

area of pyrite likely contributed to 5,000% higher concentrations of H<sub>2</sub>O<sub>2</sub> than the silicates when normalised to mass (Figure 2). However, when normalised to surface area, the H<sub>2</sub>O<sub>2</sub> concentrations from pyrite are in the same order of magnitude as those from silicates (max of 36.7 nmol m<sup>-2</sup> compared to a mean of 16.1 nmol m<sup>-2</sup> from the silicates). Therefore, the ease with which pyrite is ground likely exposes large fractured mineral surfaces in subglacial systems, resulting in enhanced mechanochemical reactions and H<sub>2</sub>O<sub>2</sub> production. Gill-Olivas et al. (2021) have previously suggested the potential for pyrite to mechanochemically generate H<sub>2</sub>O<sub>2</sub> in subglacial sediments. We show here for the first time that crushing pure pyrite has the potential to generate at least an order of magnitude more H<sub>2</sub>O<sub>2</sub> than silicate rocks and minerals for the same energy input (500 rpm, 30 min), supporting the theory that pyrite is a key mineralogical control on subglacial ecosystems (Mitchell et al., 2013; Gill-Olivas et al., 2021). However, our H<sub>2</sub>O<sub>2</sub> concentrations generated from crushed pure pyrite (mean of 0.6 μmol g<sup>-1</sup> after 1 h at 0 °C) were far lower than those generated from crushed subglacial Lake Whillans sediment (15 μmol g<sup>-1</sup>) using a similar energy input during crushing (500 rpm for 30 min). Adjusting for the pyrite content of subglacial sediments (0.56% at Robertson Glacier; Mitchell et al., 2013), we predict that pyrite can only produce 3.4 nmol H<sub>2</sub>O<sub>2</sub> per gramme of sediment, only 0.02% of the concentrations recorded by Gill-Olivas et al. (2021). We note that Gill-Olivas et al. (2021) did not measure surface area and had a higher rock–water ratio, limiting an accurate quantitative comparison. In addition, the sediment load in Gill-Olivas et al. (2021) was much lower at 15 g than at 45 g, which may have affected the grinding intensity and consequent surface area generation. However, the discrepancy in H<sub>2</sub>O<sub>2</sub> concentrations may be explained by the difference in sampling times in the experiments. H<sub>2</sub>O<sub>2</sub> production from pyrite occurs in <1 min (Borda et al., 2003), and Gill-Olivas et al. (2021) measured H<sub>2</sub>O<sub>2</sub> production after 2 min, whereas we measured H<sub>2</sub>O<sub>2</sub> only after 1 h. As indicated by the high concentration of aqueous Fe<sup>2+</sup> in our crushed pyrite experiments (reaching 38 μmol g<sup>-1</sup>) and its ratio to Fe<sup>3+</sup> (Figure 3), we suggest that Fenton reactions (Fubini and Hubbard, 2003; Eq. 10) may have removed up to 14 μmol g<sup>-1</sup> H<sub>2</sub>O<sub>2</sub> before the 1-h time point. Data from Borda et al. (2001) further support this theory as they produced 8.5 μmol g<sup>-1</sup> H<sub>2</sub>O<sub>2</sub> after 2 min from crushed pyrite crystals (unknown crushing intensity; Borda et al., 2001), much closer to the values recorded by Gill-Olivas et al. (2021). The fact that our subglacial sediment-adjusted H<sub>2</sub>O<sub>2</sub> concentrations are lower than those of Gill-Olivas et al. (2021) could therefore be interpreted as the residual concentration following its initial production and subsequent rapid destruction (Edgar et al., 2022). Alternatively, the H<sub>2</sub>O<sub>2</sub> assay may not have measured all of the H<sub>2</sub>O<sub>2</sub> generated during the experiments. We note that pH was not measured in this study due to low sample volumes; it is possible that the crushing and dissolution of pyrite generated sufficiently low pH values (< pH 5) to slow the formation of the 2Cu(DMP)<sub>2</sub><sup>+</sup> colorimetric complex used to assay H<sub>2</sub>O<sub>2</sub> (Baga et al., 1988). We note that additional investigations of H<sub>2</sub>O<sub>2</sub> generation from pyrite over shorter time periods with a variety of complimentary methods to analyse H<sub>2</sub>O<sub>2</sub> revealed no

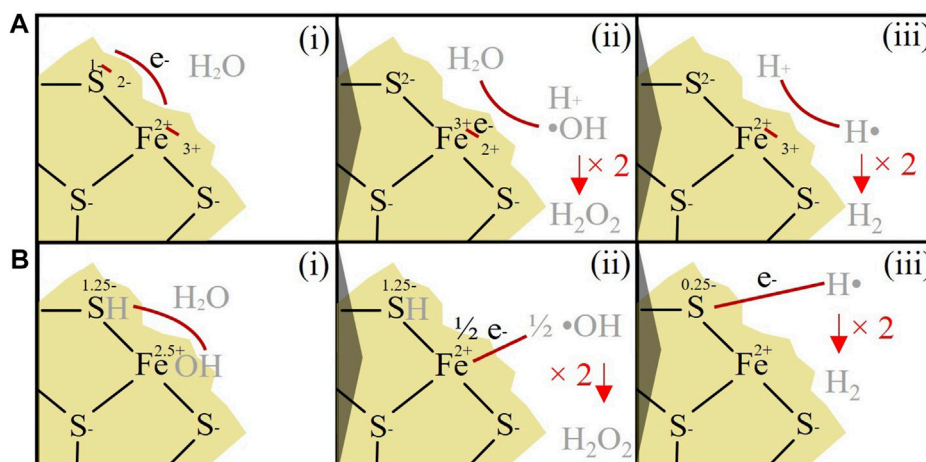


**FIGURE 4**

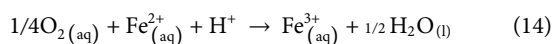
$\text{H}_2\text{O}_2$  and  $\text{H}_2$  production from the surface of crushed pyrite **(A)** i) In this model (based on Borda et al., 2003), it is assumed that the defect S site has an initial redox state of  $-2$ , and Fe, a redox state of  $+2$ .  $\text{Fe}^{2+}$  is oxidised to  $\text{Fe}^{3+}$  via the transfer of an electron to the adjacent S site. ii)  $\bullet\text{OH}$  and  $\text{H}^+$  are generated from the reaction of water with surface-bound  $\text{Fe}^{3+}$ , which reduce  $\text{Fe}^{3+}$  back to  $\text{Fe}^{2+}$ . Two  $\bullet\text{OH}$  can then react together to generate  $\text{H}_2\text{O}_2$ . iii)  $2\text{H}^+$  react with  $\text{Fe}^{2+}$  to reform  $\text{Fe}^{3+}$  at the pyrite surface and generate  $\text{H}_2$ . **(B)** i) In this model (based on Xian et al., 2019), it is assumed that the S defect site has an initial redox state of  $-1.25$ , and the Fe site has a redox state of  $+2.5$ . Water is adsorbed on the surface and split, generating  $\text{FeOH}$  and  $\text{SH}$ . ii) Electrons are transferred from the OH group to the  $\text{Fe}^{2.5+}$  sites, resulting in surface-bound  $\text{Fe}^{2+}$  and  $\bullet\text{OH}$  (note that two  $\text{Fe}^{2.5+}$  defect sites would have to be reduced to generate one  $\bullet\text{OH}$ ). Two  $\bullet\text{OH}$  then react together to generate  $\text{H}_2\text{O}_2$ . iii) The  $\text{S}^{1.25-}$  site donates an electron to H, resulting in the release of  $\text{H}\bullet$ . Two  $\text{H}\bullet$  can then react to form  $\text{H}_2$ .

relationship between the pyrite content of crushed rock and  $\text{H}_2\text{O}_2$  generation potential (Gill-Olivas et al., 2022).

### 4.3 $\text{Fe}^{2+}$ generation from crushed pyrite

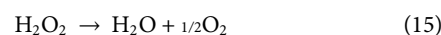
Although some  $\text{Fe}^{2+}$  may have reacted with  $\text{H}_2\text{O}_2$ , substantial concentrations of  $\text{Fe}^{2+}$  were analysed from crushed pyrite experiments (mean of  $21 \mu\text{mol g}^{-1}$ ; Supplementary Figure S4). This source of  $\text{Fe}^{2+}$  may help explain the presence of iron oxyhydroxide particles in subglacial systems, which are thought to form from the oxidation of  $\text{Fe}^{2+}$  (Hawkings et al., 2014; Nixon et al., 2017). In such systems, assuming a typical pyrite content in subglacial sediments of 0.56% (Mitchell et al., 2013),  $121 \text{ nmol}$  of  $\text{Fe}^{2+}$  can be released per gramme of sediment, based on 0.56% of the average  $\text{Fe}^{2+}$  generation from pyrite after 24 h and excluding 168 h as the  $\text{Fe}^{2+}$  concentration is likely to have decreased due to Fenton reactions (Fenton, 1894; Edgar et al., 2022).

Subglacial microorganisms such as *Sideroxydans* sp. and *Thiobacillus* sp. (Mitchell et al., 2013; Boyd et al., 2014) can utilise this  $\text{Fe}^{2+}$  as an electron donor—for example, coupled to  $\text{O}_2$  as an electron acceptor, with a Gibbs free energy of reaction ( $\Delta G_r^\circ$ ) =  $-52.2 \text{ kJ mol}^{-1}$  using standard Gibbs free energies of formation at  $2^\circ\text{C}$  (Amend and Shock, 2001) based on Eq. 14 (Boyd et al., 2014).



Theoretically,  $\text{H}_2\text{O}_2$  generated during mechanochemical reactions (Figure 2) could be used as a source of  $\text{O}_2$  even in habitats isolated from atmospheric  $\text{O}_2$  as many microorganisms (including subglacial microorganisms; Kayani et al., 2018) contain

ROS defence enzymes such as catalase. Catalase protects microbes from potentially toxic  $\text{H}_2\text{O}_2$  by disproportioning it to  $\text{H}_2\text{O}$  and  $\text{O}_2$  (Eq. 15; George, 1947).

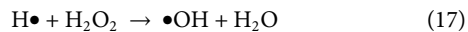
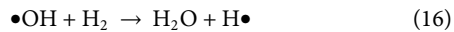


Under glaciers, Fe-utilising microbes may use this  $\text{H}_2\text{O}_2$ -derived  $\text{O}_2$ , or possibly even  $\text{H}_2\text{O}_2$  directly if any microorganisms have evolved the ability to use  $\text{H}_2\text{O}_2$  as an electron acceptor (Khademian and Imlay, 2017), to couple with the  $\text{Fe}^{2+}$  released from pyrite (Boyd et al., 2014).

### 4.4 $\text{H}_2$ generation from crushed pyrite

Our experimental data also demonstrate for the first time that pure crushed pyrite can produce  $\text{H}_2$  under low- $\text{O}_2$  conditions (Figure 3). The mechanism is unlikely to involve the oxidation of dissolved  $\text{Fe}^{2+}$  (e.g., Murray et al., 2020), as  $\text{Fe}^{2+}$  concentrations were not significantly ( $p < 0.05$ ) correlated with  $\text{H}_2$ . The  $\text{H}_2$  generated from crushed pyrite surfaces could instead potentially involve the oxidation of surface-bound  $\equiv\text{Fe}^{2+}$  linked to the reduction of  $\text{H}^+$  or water (Figure 4A), as observed for  $\text{Fe}^{2+}$ -containing silicates (Parkes et al., 2007; Mayhew et al., 2013; Okland et al., 2014; Edgar et al., 2022). However, the thermodynamic feasibility of the  $\equiv\text{Fe}^{2+}$  oxidation step is unclear. A second alternative pathway could be the reduction of adsorbed water by surface S defect sites (Figure 4B). Although steps 4bi. and 4bii. are well supported by experimental and modelling data (Xian et al., 2019), the thermodynamic feasibility of the final electron transfer from

the S defect sites to H (4Biii.) is again uncertain and would require further testing. Although the mechanism for H<sub>2</sub> generation is therefore uncertain, it is clear from **Figure 2B** that there are also additional mechanisms that remove H<sub>2</sub>. This can be explained by the reaction of H<sub>2</sub> with •OH formed at the surface of the pyrite (i.e., the Allen chain reaction; Eq. 16; Eq. 17; Edgar et al., 2022; Allen et al., 1952).



Flash heating to 30 °C also generated higher H<sub>2</sub> concentrations (**Figure 2**), presumably via an increased rate of oxidation of Fe<sup>2+</sup>. Small bursts of H<sub>2</sub> may therefore be generated as glaciers slip and release energy, temporarily raising temperatures (**Figure 1**). As mentioned above, assuming a typical pyrite concentration of 0.56% in subglacial systems and using the same calculation as with Fe<sup>2+</sup>, there can be a release of 0.26 nmol of H<sub>2</sub> per gramme of sediment. H<sub>2</sub> generation from pyrite is therefore likely to be negligible for subglacial ecosystems when compared to silicates such as granite, which are more abundant and produce more H<sub>2</sub> per gramme (**Figure 2**).

## 5 Conclusion

H<sub>2</sub> generation from crushed rock–water reactions has previously been shown to occur at temperatures relevant to subglacial environments (0 °C). However, we demonstrated that rapid increases to even moderate temperatures that might be expected at grinding sites during a glacier slip (30°C–60 °C) can increase the rate of H<sub>2</sub> production by up to 1500% over 24 h. In addition, heating to high temperatures (121 °C, potentially expected at sites where glaciers fracture rock) may have the potential to produce rapid bursts of H<sub>2</sub> in subglacial ecosystems. Most importantly, our data indicate that pyrite is likely to be a more significant source of mechanochemically generated H<sub>2</sub>O<sub>2</sub> and Fe<sup>2+</sup> than silicate minerals under glaciers. The release of Fe<sup>2+</sup> and H<sub>2</sub>O<sub>2</sub> (with the use of catalase to generate O<sub>2</sub>) could provide additional electron donors and acceptors for subglacial microbial communities. These mechanochemical energy sources may not only be relevant to subglacial ecosystems but could alter the geochemistry and potentially help support life in other cold subsurface environments that experience fluctuating temperatures, potentially including shallow subseafloor sediments and the subsurface oceans of icy moons.

## Data availability statement

The original contributions presented in the study are publicly available. This data can be found here: Telling, J. (2023). Crushed rock-water experimental data investigating the role of flash heating in hydrogen and hydrogen peroxide from silicate rocks and pyrite. NERC EDS National Geoscience Data Centre. (Dataset). <https://doi.org/10.5285/d71310b7-e5af-4979-be0c-7640d5fd71e9>.

## Author contributions

JS performed the majority of the laboratory work, helped design the detailed methods, conducted data analyses and initial interpretations, prepared figures, and co-wrote the manuscript. JE aided with the development of theories and concepts for the project and discussion, aided in chemical analyses, and contributed to the manuscript. JR assisted with chemical analyses, laboratory preparations, and initial interpretations. BG-O performed the surface area analysis. MT contributed to the manuscript. JG conducted the XRD analysis. CX assisted with XRD analysis. JT conceived the project idea and overall methodology, supervised the laboratory work, conducted some of the laboratory work, and co-wrote the manuscript.

## Funding

This research was supported by the United Kingdom Space Agency Aurora grants ST/R001421/1 and ST/S001484/1 (to JT), and NERC grants NE/S001670/1 (to MT and JT) and NE/W005506/1 (to JT).

## Acknowledgments

The authors thank Alex Charlton for assistance with HPLC analyses, Lisa Deveaux-Robinson and Dave Earley for technical assistance in the laboratories, and Ana Contessa for assistance with grain size analysis.

## Conflict of interest

The authors BG-O and JT declare that they were editorial board members of *Frontiers* at the time of submission. This had no impact on the peer review process or the final decision.

The remaining authors declare that the research was conducted in the absence of any commercial or financial relationships that could be construed as a potential conflict of interest.

## Publisher's note

All claims expressed in this article are solely those of the authors and do not necessarily represent those of their affiliated organizations, or those of the publisher, the editors and the reviewers. Any product that may be evaluated in this article, or claim that may be made by its manufacturer, is not guaranteed or endorsed by the publisher.

## Supplementary material

The Supplementary Material for this article can be found online at: <https://www.frontiersin.org/articles/10.3389/fgeoc.2023.1180893/full#supplementary-material>

## References

- Allen, A. O., Hochanadel, C., Ghormley, J., and Davis, T. (1952). Decomposition of water and aqueous solutions under mixed fast neutron and  $\Gamma$ -radiation. *J. Phys. Chem.* 56, 575–586. doi:10.1021/j150497a007
- Amend, J. P., and Shock, E. L. (2001). Energetics of overall metabolic reactions of thermophilic and hyperthermophilic archaea and bacteria. *Fems Microbiol. Rev.* 25, 175–243. doi:10.1111/j.1574-6976.2001.tb00576.x
- Araujo, F., Yokoyama, L., Teixeira, L., and Campos, J. (2011). Heterogeneous fenton process using the mineral hematite for the discoloration of a reactive dye solution. *Braz. J. Chem. Eng.* 28, 605–616. doi:10.1590/S0104-66322011000400006
- Baga, A. N., Johnson, G. A., Nazhat, N. B., and Saadalla-Nazhat, R. A. (1988). A simple spectrophotometric determination of hydrogen peroxide at low concentrations in aqueous solution. *Anal. Chim. Acta* 204, 349–353. doi:10.1016/S0003-2670(00)86374-6
- Bardestani, R., Patience, G. S., and Kaliaguine, S. (2019). Experimental methods in chemical engineering: Specific surface area and pore size distribution measurements—bet, bjh, and dft. *Can. J. Chem. Eng.* 97, 2781–2791. doi:10.1002/cjce.23632
- Benn, D. I., Jones, R. L., Luckman, A., Fürst, J. J., Hewitt, I., and Sommer, C. (2019). Mass and enthalpy budget evolution during the surge of a polythermal glacier: A test of theory. *J. Of Glaciol.* 65, 717–731. doi:10.1017/jog.2019.63
- Bindschadler, R. A., King, M. A., Alley, R. B., Anandakrishnan, S., and Padman, L. (2003). Tidally controlled stick-slip Discharge of a west antarctic ice. *Science* 301, 1087–1089. doi:10.1126/science.1087231
- Borda, M. J., Elsetinow, A. R., Schoonen, M. A., and Strongin, D. R. (2001). Pyrite-induced hydrogen peroxide formation as a driving force in the evolution of photosynthetic organisms on an early earth. *Astrobiology* 1, 283–288. doi:10.1089/15311070152757474
- Borda, M. J., Elsetinow, A. R., Strongin, D. R., and Schoonen, M. A. (2003). A mechanism for the production of hydroxyl radical at surface defect sites on pyrite. *Geochimica Cosmochimica Acta* 67, 935–939. doi:10.1016/S0016-7037(02)01222-X
- Boyd, E. S., Hamilton, T. L., Havig, J. R., Skidmore, M. L., and Shock, E. L. (2014). Chemolithotrophic primary production in a subglacial ecosystem. *Appl. And Environ. Microbiol.* 80, 6146–6153. doi:10.1128/AEM.01956-14
- Buckley, A., and Woods, R. (2015). Can sulfide minerals oxidize water to hydrogen peroxide during grinding in the absence of dissolved oxygen? *Min. Metallurgy Explor.* 32, 59–61. doi:10.1007/BF03402358
- Christner, B. C., Priscu, J. C., Achberger, A. M., Barbante, C., Carter, S. P., Christianson, K., et al. (2014). A microbial ecosystem beneath the west antarctic ice sheet. *Nature* 512, 310–313. doi:10.1038/nature13667
- Cook, S. J., Swift, D. A., Kirkbride, M. P., Knight, P. G., and Waller, R. I. (2020). The empirical basis for modelling glacial erosion rates. *Nat. Commun.* 11, 759. doi:10.1038/s41467-020-14583-8
- Edgar, J. O., Gilmour, K., White, M. L., Abbott, G. D., and Telling, J. (2022). Aeolian driven oxidant and hydrogen generation in martian regolith: The role of mineralogy and abrasion temperature. *Earth And Planet. Sci. Lett.* 579, 117361. doi:10.1016/j.epsl.2021.117361
- Fenton, H. J. H. (1894). Lxxiii.—oxidation of tartaric acid in presence of iron. *J. Of Chem. Soc. Trans.* 65, 899–910. doi:10.1039/CT8946500899
- Fischer, L., Huggel, C., Käab, A., and Haeblerli, W. (2013). Slope failures and erosion rates on a glacierized high-mountain face under climatic changes. *Earth Surf. Process. Landforms* 38, 836–846. doi:10.1002/esp.3355
- Fischer, U. H., and Clarke, G. K. (1997). Stick-slip sliding behaviour at the base of a glacier. *Ann. Of Glaciol.* 24, 390–396. doi:10.3189/S026030500012490
- Fubini, B., Bolis, V., and Giamello, E. (1987). The surface chemistry of crushed quartz dust in relation to its pathogenicity. *Inorganica Chim. Acta* 138, 193–197. doi:10.1016/S0020-1693(00)81222-0
- Fubini, B., Giamello, E., Volante, M., and Bolis, V. (1990). Chemical functionalities at the silica surface determining its reactivity when inhaled. Formation and reactivity of surface radicals. *Toxicol. And Industrial Health* 6, 571–598.
- Fubini, B., and Hubbard, A. (2003). Reactive oxygen species (ROS) and reactive nitrogen species (RNS) generation by silica in inflammation and fibrosis. *Free Radic. Biol. And Med.* 34, 1507–1516. doi:10.1016/s0891-5849(03)00149-7
- George, P. (1947). Reaction between catalase and hydrogen peroxide. *Nature* 160, 41–43. doi:10.1038/160041a0
- Gill Olivas, B. (2019). *Rock comminution of Subglacial Lake sediments as a potential source of energy and nutrients to the Subglacial Lake Whillans microbial ecosystem*. PhD thesis. University of Bristol.
- Gill-Olivas, B., Telling, J., Skidmore, M., and Tranter, M. (2022). Abrasion of sedimentary rocks as a source of hydrogen peroxide and nutrients to subglacial ecosystems. *Egusphere*, 1–21. doi:10.5194/egusphere-2022-908
- Gill-Olivas, B., Telling, J., Tranter, M., Skidmore, M., Christner, B., O'doherty, S., et al. (2021). Subglacial erosion has the potential to sustain microbial processes in Subglacial Lake Whillans, Antarctica. *Commun. Earth Environ.* 2, 134–212. doi:10.1038/s43247-021-00202-x
- Hart, J. K., Rose, K. C., and Martinez, K. (2011). Subglacial till behaviour derived from *in situ* wireless multi-sensor subglacial probes: Rheology, hydro-mechanical interactions and till formation. *Quat. Sci. Rev.* 30, 234–247. doi:10.1016/j.quascirev.2010.11.001
- Hawkings, J. R., Wadhams, J. L., Tranter, M., Raiswell, R., Benning, L. G., Statham, P. J., et al. (2014). Ice sheets as a significant source of highly reactive nanoparticulate iron to the oceans. *Nat. Commun.* 5, 3929–3938. doi:10.1038/ncomms4929
- He, H., Wu, X., Xian, H., Zhu, J., Yang, Y., Lv, Y., et al. (2021). An abiotic source of archaic hydrogen peroxide and oxygen that pre-dates oxygenic photosynthesis. *Nat. Commun.* 12, 6611. doi:10.1038/s41467-021-26916-2
- He, H., Wu, X., Zhu, J., Lin, M., Lv, Y., Xian, H., et al. (2023). A mineral-based origin of Earth's initial hydrogen peroxide and molecular oxygen. *Proc. Natl. Acad. Sci. U. S. A.* 120, e2221984120. doi:10.1073/pnas.2221984120
- Irfan, M., Zhou, L., Bai, Y., Yuan, S., Liang, T.-T., Liu, Y.-F., et al. (2019). Insights into the hydrogen generation from water-iron rock reactions at low temperature and the key limiting factors in the process. *Int. J. Hydrogen Energy* 44, 18007–18018. doi:10.1016/j.ijhydene.2019.05.086
- Kaur, J., Rickman, D., and Schoonen, M. A. (2016). Reactive oxygen species (ROS) generation by lunar simulants. *Acta Astronaut.* 122, 196–208. doi:10.1016/j.actaastro.2016.02.002
- Kayani, M., Doyle, S. M., Sangwan, N., Wang, G., Gilbert, J. A., Christner, B. C., et al. (2018). Metagenomic analysis of basal ice from an Alaskan glacier. *Microbiome* 6, 123. doi:10.1186/s40168-018-0505-5
- Khademian, M., and Inlay, J. A. (2017). Escherichia coli cytochrome C peroxidase is a respiratory oxidase that enables the use of hydrogen peroxide as a terminal electron acceptor. *Proc. Natl. Acad. Sci. U. S. A.* 114, E6922–E6931. doi:10.1073/pnas.1701587114
- Kita, I., Matsuo, S., and Wakita, H. (1982). H<sub>2</sub> generation by reaction between H<sub>2</sub>O and crushed rock: An experimental study on H<sub>2</sub> degassing from the active fault zone. *J. Geophys. Res. Solid Earth* 87, 10789–10795. doi:10.1029/JB087IB13P10789
- Macdonald, M. L., Wadhams, J. L., Telling, J., and Skidmore, M. L. (2018). Glacial erosion liberates lithologic energy sources for microbes and acidity for chemical weathering beneath glaciers and ice sheets. *Front. Earth Sci.* 6, 212. doi:10.3389/feart.2018.00212
- Mayhew, L. E., Ellison, E., McCollom, T., Trainor, T., and Templeton, A. (2013). Hydrogen generation from low-temperature water-rock reactions. *Nat. Geosci.* 6, 478–484. doi:10.1038/ngeo1825
- McCollom, T. M., and Bach, W. (2009). Thermodynamic constraints on hydrogen generation during serpentinization of ultramafic rocks. *Geochimica Cosmochimica Acta* 73, 856–875. doi:10.1016/j.gca.2008.10.032
- McCollom, T. M., and Donaldson, C. (2016). Generation of hydrogen and methane during experimental low-temperature reaction of ultramafic rocks with water. *Astrobiology* 16, 389–406. doi:10.1089/ast.2015.1382
- Mitchell, A. C., Lafrenière, M. J., Skidmore, M. L., and Boyd, E. S. (2013). Influence of bedrock mineral composition on microbial diversity in a subglacial environment. *Geology* 41, 855–858. doi:10.1130/g34194.1
- Murray, J., Clément, A., Fritz, B., Schmittbuhl, J., Bordmann, V., and Fleury, J. M. (2020). Abiotic hydrogen generation from biotite-rich granite: A case study of the soultz-sous-forêts geothermal site, France. *Appl. Geochem.* 119, 104631. doi:10.1016/j.apgeochem.2020.104631
- Nixon, S. L., Telling, J. P., Wadhams, J. L., and Cockell, C. S. (2017). Viable cold-tolerant iron-reducing microorganisms in geographically diverse subglacial environments. *Biogeosciences* 14, 1445–1455. doi:10.5194/bg-14-1445-2017
- Oklund, I., Huang, S., Thorseth, I., and Pedersen, R. (2014). formation of H<sub>2</sub>, CH<sub>4</sub> and N-species during low-temperature experimental alteration of ultramafic rocks. *Chem. Geol.* 387, 22–34. doi:10.1016/j.chemgeo.2014.08.003
- Parkes, R. J., Berlendis, S., Roussel, E. G., Bahruji, H., Webster, G., Oldroyd, A., et al. (2019). Rock-crushing derived hydrogen directly supports a methanogenic community: Significance for the deep biosphere. *Environ. Microbiol. Rep.* 11, 165–172. doi:10.1111/1758-2229.12723
- Parkes, R. J., Linnane, C. D., Webster, G., Sass, H., Weightman, A. J., Hornibrook, E. R., et al. (2011). Prokaryotes stimulate mineral H<sub>2</sub> formation for the deep biosphere and subsequent thermogenic activity. *Geology* 39, 219–222. doi:10.1130/G31598.1
- Parkes, R. J., Wellsbury, P., Mather, I. D., Cobb, S. J., Cragg, B. A., Hornibrook, E. R., et al. (2007). Temperature activation of organic matter and minerals during burial has the potential to sustain the deep biosphere over geological timescales. *Org. Geochem.* 38, 845–852. doi:10.1016/j.orggeochem.2006.12.011
- Schoonen, M. A., Harrington, A. D., Laffers, R., and Strongin, D. R. (2010). Role of hydrogen peroxide and hydroxyl radical in pyrite oxidation by molecular oxygen. *Geochimica Cosmochimica Acta* 74, 4971–4987. doi:10.1016/j.gca.2010.05.028

- Sevestre, H., and Benn, D. I. (2015). Climatic and geometric controls on the global distribution of surge-type glaciers: Implications for a unifying model of surging. *J. Of Glaciol.* 61, 646–662. doi:10.3189/2015jg14j136
- Stone, J., Edgar, J., Gould, J., and Telling, J. (2022). Tectonically-driven oxidant production in the hot biosphere. *Nat. Commun.* 13, 4529–4610. doi:10.1038/s41467-022-32129-y
- Telling, J., Boyd, E., Bone, N., Jones, E., Tranter, M., Macfarlane, J., et al. (2015). Rock comminution as a source of hydrogen for subglacial ecosystems. *Nat. Geosci.* 8, 851–855. doi:10.1038/ngeo2533
- Ueki, R., Imaizumi, Y., Iwamoto, Y., Sakugawa, H., and Takeda, K. (2020). Factors controlling the degradation of hydrogen peroxide in river water, and the role of riverbed sand. *Sci. Total Environ.* 716, 136971. doi:10.1016/j.scitotenv.2020.136971
- Viollier, E., Inglett, P., Hunter, K., Roychoudhury, A., and Van Cappellen, P. (2000). The ferrozine method revisited: Fe (II)/Fe (III) determination in natural waters. *Appl. Geochem.* 15, 785–790. doi:10.1016/S0883-2927(99)00097-9
- Wadham, J. L., Tranter, M., Tulaczyk, S., and Sharp, M. (2008). Subglacial methanogenesis: A potential climatic amplifier? *Glob. Biogeochem. Cycles* 22, 22. doi:10.1029/2007GB002951
- Xian, H., Zhu, J., Tan, W., Tang, H., Liu, P., Zhu, R., et al. (2019). The mechanism of defect induced hydroxylation on pyrite surfaces and implications for hydroxyl radical generation in prebiotic chemistry. *Geochimica Cosmochimica Acta* 244, 163–172. doi:10.1016/j.gca.2018.10.009
- Yi, J., Bahrini, C., Schoemaeker, C., Fittschen, C., and Choi, W. (2012). Photocatalytic decomposition of H<sub>2</sub>O<sub>2</sub> on different TiO<sub>2</sub> surfaces along with the concurrent generation of HO<sub>2</sub> radicals monitored using cavity ring down spectroscopy. *J. Phys. Chem. C* 116, 10090–10097. doi:10.1021/jp301405e
- Zhang, P., Yuan, S., and Liao, P. (2016). Mechanisms of hydroxyl radical production from abiotic oxidation of pyrite under acidic conditions. *Geochimica et Cosmochimica Acta* 172, 444–457. doi:10.1016/j.gca.2015.10.015
- Zhang, S., and Valentine, J. M. (2002). Stick-slip and temperature effect in the scratching of materials. *Tribol. Lett.* 12, 195–202. doi:10.1023/A:1015453725893